



## RESEARCH LETTER

10.1002/2017GL073572

## Key Points:

- Tropical cyclones generate gravity waves that radiate outward as tight spirals
- The waves can be identified in aircraft observations and from surface instruments
- Numerical simulations suggest that wave amplitude can be related to TC intensity

## Supporting Information:

- Supporting Information S1
- Movie S1

## Correspondence to:

D. S. Nolan,  
dnolan@rsmas.miami.edu

## Citation:

Nolan, D. S., and J. A. Zhang (2017), Spiral gravity waves radiating from tropical cyclones, *Geophys. Res. Lett.*, *44*, 3924–3931, doi:10.1002/2017GL073572.

Received 23 MAR 2017

Accepted 12 APR 2017

Accepted article online 18 APR 2017

Published online 30 APR 2017

## Spiral gravity waves radiating from tropical cyclones

David S. Nolan<sup>1</sup>  and Jun A. Zhang<sup>2,3</sup> 

<sup>1</sup>Department of Atmospheric Sciences, University of Miami, Miami, Florida, USA, <sup>2</sup>Hurricane Research Division, NOAA/AOML, Miami, Florida, USA, <sup>3</sup>Cooperative Institute for Marine and Atmospheric Sciences, University of Miami, Miami, Florida, USA

**Abstract** Internal gravity waves are continuously generated by deep moist convection around the globe. Satellite images suggest that tropical cyclones produce short-wavelength, high-frequency waves that radiate outward, with the wave fronts wrapped into tight spirals by the large differential advection of the sheared tangential flow. This letter presents new in situ observations of such waves from two sources: flight level data from research aircraft that show radial wavelengths of 2–10 km and vertical velocity magnitudes from 0.1 to 1.0 ms<sup>-1</sup> and surface observations from a research buoy in the Pacific that indicate the passage of gravity waves overhead as tropical cyclones pass by at distances of 100 to 300 km. Numerical simulations are used to interpret these observations and to understand the broader horizontal and vertical structures of the radiating waves. The simulations suggest a correlation between wave amplitude and cyclone intensity, which could be used to make remote estimates of peak wind speeds.

**Plain Language Summary** Thunderstorms in the cores of tropical cyclones generate waves that radiate outward in expanding spiral patterns. These waves can be detected in satellite images, from aircraft, and even surface instruments. They could potentially be used to monitor cyclone intensity from long distances.

## 1. Introduction

Internal waves in the atmosphere, also known as gravity waves, exist due to the natural restoring force associated with the static stability of the atmosphere [Markowski and Richardson, 2010; Sutherland, 2010]. Significant gravity wave generation is associated with three processes: the interaction of the atmospheric flow with topography, rapidly evolving imbalances of the large-scale flow, and disruptions to the atmosphere by moist convection. Gravity waves play a critical role in the dynamical adjustment processes that keep the atmosphere close to hydrostatic and geostrophic wind balance, by redistributing localized heating over larger distances, up to the scale of the Rossby deformation radius [e.g., Vallis, 2006, section 3.8].

While the transfer of moist enthalpy from the ocean to the atmosphere is the ultimate energy source for tropical cyclones (TCs) [Emanuel, 1991], deep moist convection near the storm center is the mechanism by which this energy is converted to heat and then to kinetic energy of the wind field [Nolan et al., 2007]. As for ordinary continental and oceanic convection, TC convection produces gravity waves that propagate both upward and outward. Clear signals of these upward propagating waves have been observed in the stratosphere, usually seen as circular or semicircular bands of temperature anomalies radiating outward from the storm center [Yue et al., 2014], occasionally with some degree of banding patterns. Simulations with mesoscale atmospheric models have reproduced these features, which generally have wavelengths of tens to hundreds of kilometers [Kim et al., 2009]. These waves propagate long distances, and their influence on the atmospheric boundary layer have also been observed [Niranjan Kumar et al., 2014].

This paper is concerned with smaller-scale waves, with radial wavelengths of 2 to 20 km, that radiate outward from the TC core with phase speeds of 20 to 30 ms<sup>-1</sup>. We show that these waves can be observed at relatively low altitudes (1.5 km–3 km) for hundreds of kilometers from the center and also that the waves induce surface pressure anomalies that can be detected at these distances. Jewtoukoff et al. [2013] reported observations near a TC of gravity waves with wavelengths as short as 1 km, but these were taken by a balloon at 19 km altitude. To our knowledge, only the atmospheric oscillations observed near a TC by Sato [1993] had similar qualities to those we present here.

Visual evidence for these waves was documented in the early study by Black [1983], who analyzed features in cloud tops using stereoscopic analysis of photographs taken from hand-held cameras on the Skylab space

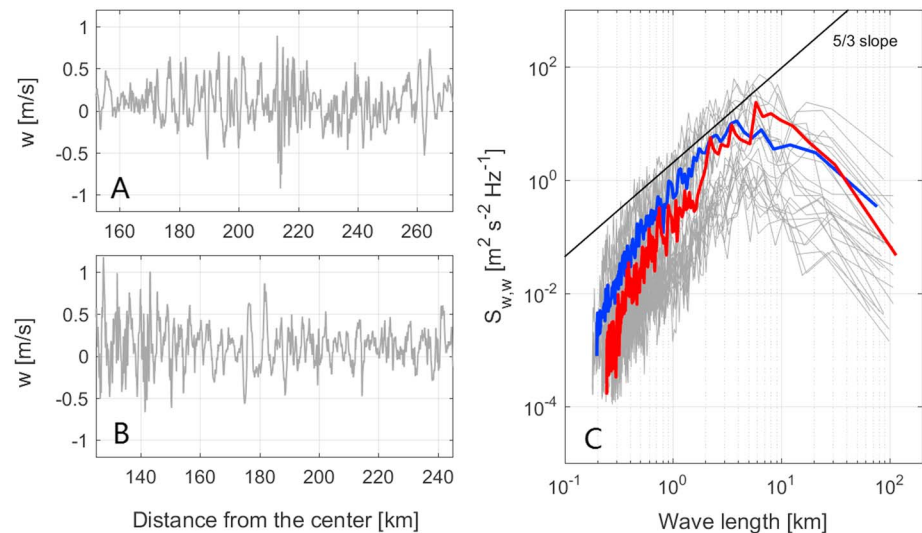


**Figure 1.** Flight level data from NOAA P3 aircraft: (a) vertical velocity ( $w$ ) observed in Hurricane Frances (2004) on 1 September 2004, with the  $x$  coordinate indicating distance from the storm center; (b) as in Figure 1a but for Hurricane Ivan (2004) on 15 September 2004; (c) Power spectra for  $w$  for 25 different flight legs over five different storms, with composite mean spectra for inbound legs (blue) and outbound legs (red). Flight altitudes are listed in Table S1.

station. He found wavelengths ranging from 2 to 18 km. As the horizontal resolution and frequency of satellite images has increased over the years, the waves have become more frequently discernible. Movie S1 in the supporting information shows an animation of visible images of Typhoon Meranti (2016) in the Pacific Ocean obtained by the Himawari 8 satellite [Japan Meteorological Agency, 2016]. Numerous spiral patterns, appearing as ripples in the thin cirrus clouds overlying the dense clouds underneath, radiate outward from the storm center. From these images we estimate that the waves have an outward phase speed of  $29 \text{ ms}^{-1}$  (details are provided in the supporting information S1). It is not possible to know how much of this motion is due to wave propagation and how much is due to advection by the upper level outflow of the storm, which can range from  $5$  to  $15 \text{ ms}^{-1}$  [Molinari *et al.*, 2014].

The purpose of this letter is to present new in situ observations of these spiral waves from aircraft data and surface instruments. Since such data provide little spatial coverage, we use numerical simulations to infer the broader horizontal and vertical structures of the waves.

## 2. Aircraft Observations

### 2.1. Flight Level Data

We consider flight level data collected by NOAA WP-3D aircraft [Aberson *et al.*, 2006] in Hurricanes Fabian (2003), Isabel (2003), Frances (2004), Ivan (2004), and Jeanne (2004) as part of the Coupled Boundary Layer Air-Sea Transfer experiment [Black *et al.*, 2007]. Additional details regarding the data and processing are provided in the supporting information S2.

### 2.2. Results

Figures 1a and 1b show examples of data from flight legs in Hurricane Frances (2004) and Hurricane Ivan (2004), each showing oscillations in vertical velocity ( $w$ ) with length scales of 2–10 km and amplitudes up to around  $1 \text{ ms}^{-1}$ . To better quantify the length scales, power spectra are computed over 25 flight legs across several storms as shown in Figure 1c. In computing the spectra, time series of  $w$  are converted to distance using the typical aircraft speed of  $110 \text{ ms}^{-1}$ , and data from the eye and eyewall region are excluded. For shorter wavelengths, the spectra follow a  $5/3$  power law, similar to atmospheric wind spectra from observations [e.g., Nastrom and Gage, 1985] and produced in numerical simulations [e.g., Durran and Weyn, 2016]. In contrast, Figure 1c shows a broad peak from 2 to 10 km, perhaps due to the excitation of short-wavelength gravity waves from nearby convection in the eyewall.

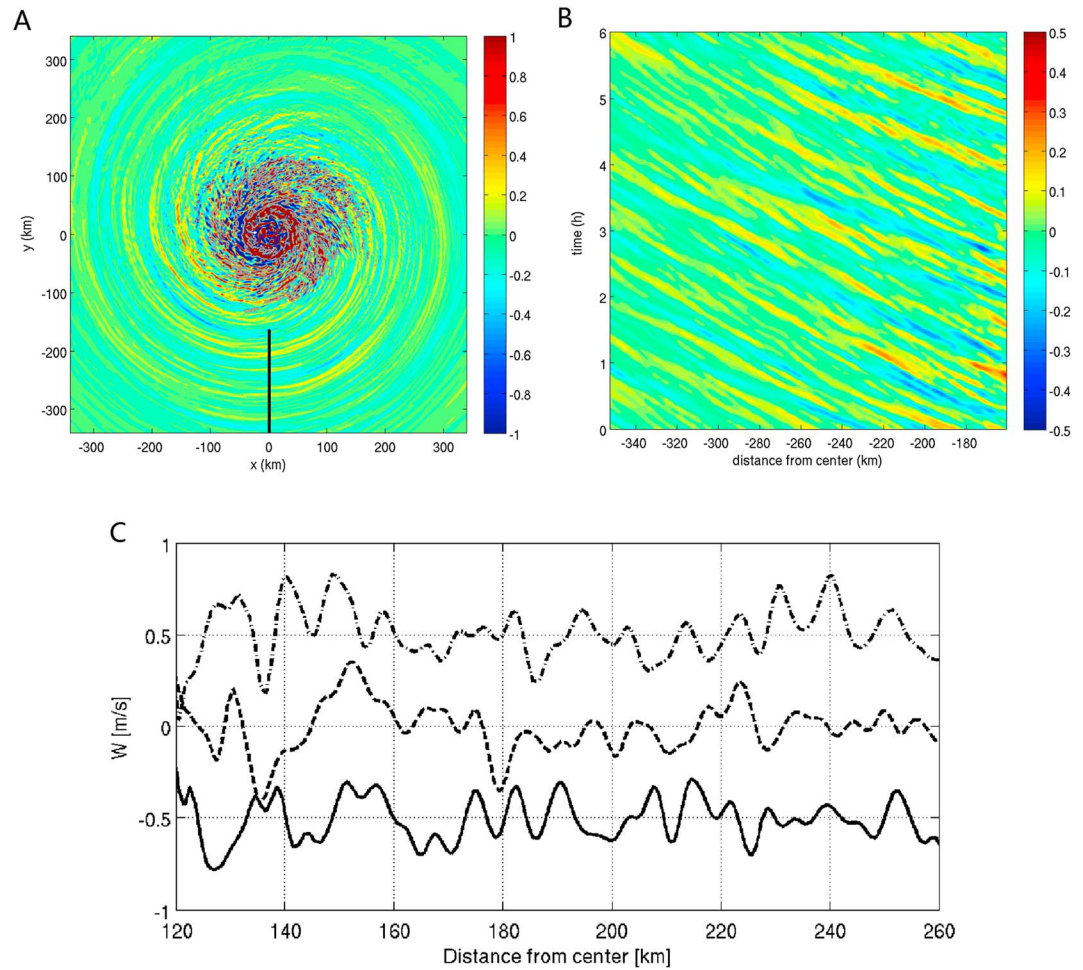


**Figure 2.** Gravity waves in an idealized TC simulation: (a) snapshot of  $w$  in  $\text{ms}^{-1}$  at 700 hPa, with color shading interval  $0.1 \text{ ms}^{-1}$  and single gray contour showing total condensate equal to  $4 \times 10^{-4} \text{ kg kg}^{-1}$ ; (b) radius-time Hovmöller diagram of  $w$  at 700 hPa along a line emanating due south of the storm center, with interval  $0.025 \text{ ms}^{-1}$ ; (c) simulated time series of  $w$  from model output for an inbound aircraft at three different start times from a point due south of the center; for easier comparison each curve is shifted by  $-0.5 \text{ ms}^{-1}$  (solid),  $0 \text{ ms}^{-1}$  (dashed), and  $0.5 \text{ ms}^{-1}$  (dash dotted).

Since the waves are themselves propagating outward, the inferred wavelengths are modified by the Doppler effect. By computing composite spectra separately for inbound and outbound legs (Figure 1c), we can estimate the phase speeds from  $C_p = S \times (\lambda_o - \lambda_i) / (\lambda_o + \lambda_i)$ , where  $S$  is the aircraft speed and  $\lambda_o$  and  $\lambda_i$  are the outbound and inbound wavelengths, respectively. From  $\lambda_o = 6 \text{ km}$ ,  $\lambda_i = 4 \text{ km}$ , and  $S = 110 \text{ ms}^{-1}$ , we estimate  $C_p = 22 \text{ ms}^{-1}$ . This phase speed is consistent with the speed crudely estimated from the satellite images above.

### 3. Numerical Simulations

#### 3.1. Modeling Framework

To better understand the horizontal and vertical structures of the waves shown above, we analyze two idealized simulations of tropical cyclones generated using version 3.4.1 of the Weather Research and Forecasting Model (WRF). The simulations use nested grids that follow the center of the storm, with 1 km grid spacing in an inner nest that is  $720 \text{ km} \times 720 \text{ km}$  in size. The background wind field has  $5 \text{ ms}^{-1}$  easterly (westward) flow with  $2.5 \text{ ms}^{-1}$  of wind shear between 850 and 200 hPa. The sea surface temperature (SST) is set to either  $26.5^\circ\text{C}$  or  $25.0^\circ\text{C}$ . Further details are provided in Text S3.

Given their favorable environments, each cyclone intensifies and reaches an approximately steady state after 5 days (for SST = 26.5°C) or 6 days (for SST = 25°C) and achieves surface winds in the range of 70–75 ms<sup>-1</sup> (hereafter, Category 5) and winds of 40–45 ms<sup>-1</sup> (hereafter, Category 2), respectively. For each simulation the full three-dimensional fields were saved every 2 min for 24 h after the approximately steady state was achieved.

### 3.2. Simulated Radiating Gravity Waves

Figure 2a shows  $w$  at pressure altitude 700 hPa (most frequently used by NOAA research aircraft that investigate TCs) for the Category 5 TC. In the core or “eyewall” region, updrafts and downdrafts well in excess of 10 ms<sup>-1</sup> penetrate upward and downward through the layer; the color scale (–1 to +1 ms<sup>-1</sup>) is saturated for these features. Outside the core, tight spirals of vertical velocity are evident. Similar spiral waves appear to be visible in the WRF simulation of *Jewtoukoff et al.* [2013, Figure 7c] but were not discussed in that paper. The gray contour in Figure 2a shows concentrations of total cloud water and rain exceeding  $4 \times 10^{-4}$  kg kg<sup>-1</sup> (5% of the maximum value at this level), indicating that active convection is confined to the eyewall and spiral bands limited to within 150 km of the center. Beyond this radius the spiral waves are decoupled from convection and are not affected by moist saturation. A radius-time Hovmöller diagram, constructed from model data along a line radiating due South from the vortex center (Figure 2b), and thus perpendicular to the storm motion, shows waves propagating outward with phase velocities of 20 to 25 ms<sup>-1</sup>, consistent with the phase speeds derived above from satellite and aircraft observations.

One way to more directly compare the observed flight level waves and those produced in the simulation is to generate time series from simulated aircraft flying through the storm. Figure 2c shows three times series of  $w$  at 700 hPa computed by interpolating the model output to a point that is moving inward toward the center at the same speed as the aircraft (110 ms<sup>-1</sup>). Not surprisingly, with 1 km horizontal grid spacing, the model cannot reproduce the same high-frequency structures as observed, but it does show waves with about half the amplitude and twice the radial wavelengths (8–12 km).

While the outward phase speeds of the observed and modeled waves agree quite well, they do not quite match phase speeds computed from the classic dispersion relation for gravity waves in a resting atmosphere,  $C_p = \omega/k = N/(k^2 + m^2)^{1/2}$ , where  $\omega$  is the wave frequency,  $N$  is the Brunt-Vaisala frequency,  $k$  is a horizontal wave number, and  $m$  is a vertical wave number. To estimate  $C_p$ , we use  $N$  computed from the model output and values of  $k$  corresponding to wavelengths of 5 to 10 km. The vertical wavelength is estimated to be 10–12 km from an analysis of the vertical structure of the waves that is provided in Text S4. These parameters lead to radial phase speeds of 10–15 ms<sup>-1</sup>. An additional 1–2 ms<sup>-1</sup> of outward phase speed can be gained from the “apparent” propagation effect due to the advection of the spiral phase lines by the tangential wind [see *Moon and Nolan*, 2015, p. 197 and Figure 8]. The faster outward speeds of the observed and simulated waves may represent the effects of the environmental flow (such as the vertical shear of the tangential wind or the upper level outflow) or simply fundamental differences in the dynamics of these spiral waves.

To better isolate the horizontal structures of the waves, we perform filtering by azimuthal wave number. Figure 3a shows the sum of asymmetric wave number components 2 to 5 of the same  $w$  field shown in Figure 2a (see Text S5 for details). This is quite similar to the original  $w$  field but retains mostly smoother radial structures. It is interesting to compare this field to the surface pressure field from the same time, filtered in the same manner (Figure 3b). The radial structures are generally broader for the surface pressure field, and there is relatively little spatial correlation between  $w$  at 700 hPa and surface pressure. This suggests that the radiating wave structures at the surface and at flight level are actually signals from two different waves, perhaps resulting from the projection of the vertical heating structures onto different internal modes. To illustrate further, Figure 3c shows time series of wave number-filtered  $w$  and surface pressure from a point 300 km south of the center. The time series are not well correlated, and spectral analysis reveals that the dominant period for variability of  $w$  is around 1000 s, whereas for surface pressure it is around 2100 s.

### 3.3. Simulated Surface Pressure and Wind Power Spectra

Gravity waves passing overhead of a fixed point at the surface can cause observable surface pressure variations [*Koch and Siedlarz*, 1999; *Stephan et al.*, 2016]. We use our simulations to assess whether or not the spiral gravity waves shown above produce signals that could be observed at the surface, even without the benefit

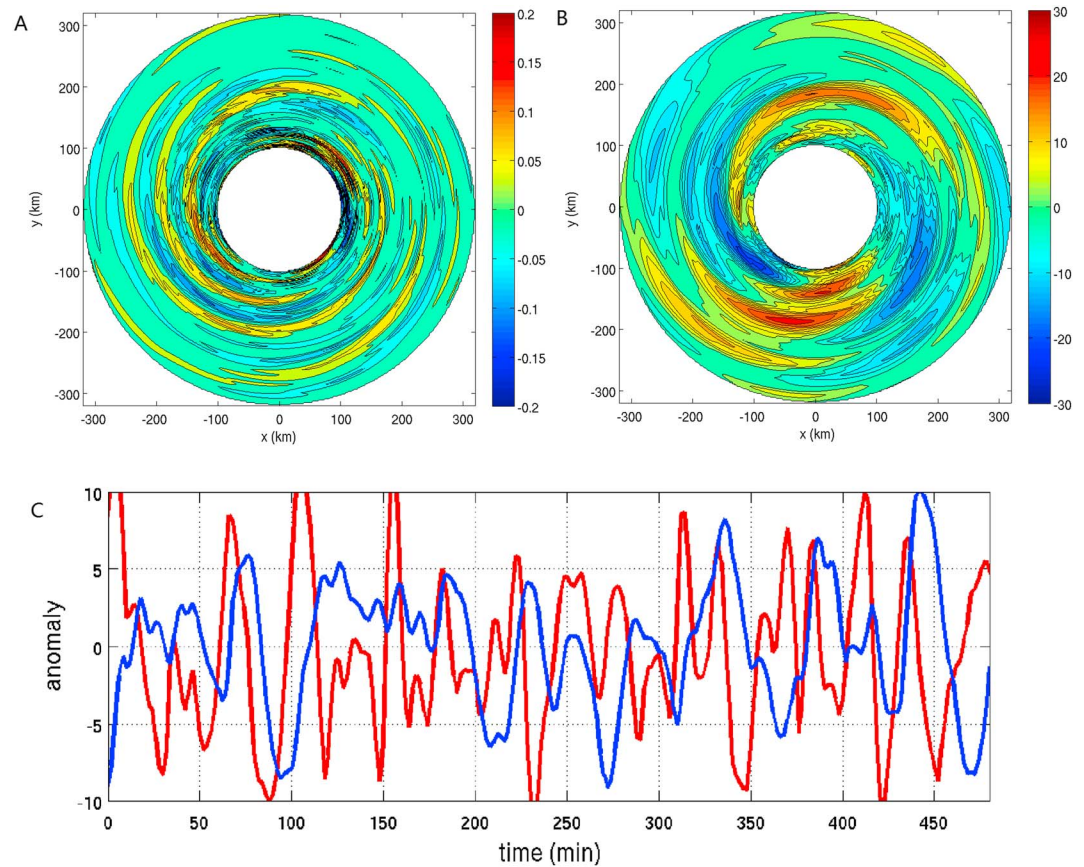


**Figure 3.** Results of wave number filtering: (a) the same  $w$  field as in Figure 2a but after filtering to retain azimuthal wave numbers 2 to 5, contour interval  $0.025 \text{ ms}^{-1}$ ; (b) the filtered surface pressure field from the same time, interval  $2.5 \text{ Pa}$ ; (c) time series of filtered  $w$  (red) and surface pressure (blue) from the point  $300 \text{ km}$  south of the cyclone center, with  $w$  in  $\text{ms}^{-1}$  multiplied by  $200$  and pressure in Pascal. Data are suppressed inside  $80 \text{ km}$  for clarity.

of the wave-filtering procedure which requires knowledge of the entire pressure field. In addition to the three-dimensional fields saved every  $2 \text{ min}$ , surface wind speed and surface pressure were also saved every  $10 \text{ s}$ . From these, we construct time series of surface variables, but unlike above, the data are interpolated to fixed points, rather than moving with the storm, so as to simulate how a surface station would record the data. Specifically, two sets of  $25$  simulated sensors are located in a  $5 \times 5$  array, separated by distances of  $10 \text{ km}$ , with one array centered  $300 \text{ km}$  to the north of the storm and the other array centered  $300 \text{ km}$  to the south. As the storm is moving nearly due west, these are the distances at the point of closest approach. Power spectra of the surface pressure and surface wind time series for each array were computed and then averaged among each set of  $25$  sensors.

These mean spectra are shown in Figure 4. The peak power for pressure oscillations is greater for the Category 5 storm than for the Category 2 storm; this is also true for wind, but the differences are not as large. Interestingly, the spectra are also different on the north and south sides of each storm, with the greatest differences occurring for shorter periods ( $100$  to  $1000 \text{ s}$ ). This increase in power at high frequencies may be related to the fact that there is more convective activity in the eyewall and rainbands on the north sides of each storm, because they are moving westward (increasing surface wind speeds on the north side) and they are both subjected to  $2.5 \text{ ms}^{-1}$  of westerly wind shear, which also increases convection on the north side (downshear left) of the eyewall [Corbosiero and Molinari, 2003]. The opposite is true at longer periods ( $1000$  to  $4000 \text{ s}$ ), with higher peaks in power observed on the south sides. The results suggest that it could be possible to use differences in surface pressure and wind spectra to infer information about the direction of motion or the convective asymmetry of a passing TC.

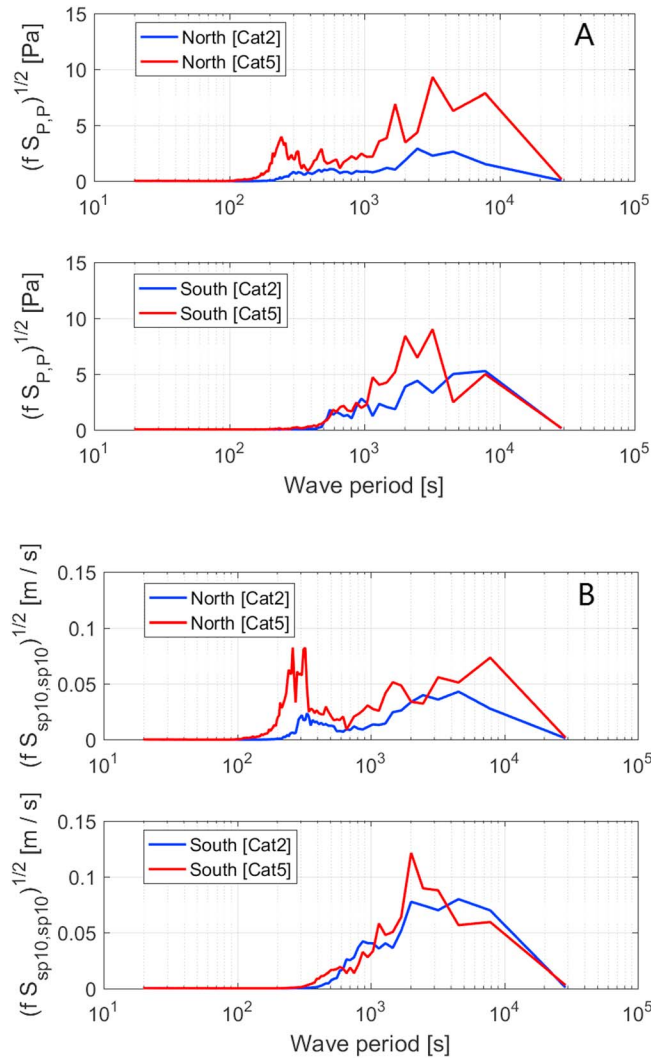


**Figure 4.** Averaged power spectra of (a) surface pressure and (b) surface wind speed, from two sets of surface instruments placed 300 km north and south of the Category 5 and Category 2 TCs. Red curves show results for the Category 5 storm and blue curves show results for the Category 2 storm.

**4.2. Buoy Data Analysis**

Figure 5 shows power spectra of the surface pressure and wind time series during the nearby passage of each typhoon, along with comparisons to power spectra from periods with no TCs. All the spectra show peaks at periods from 800 to 1200 s, or 2000 to 3000 s, or both. These periods are longer than those of the strongest waves observed at flight level (about 230 s, based on the wavelength and phase speed analyzed in section 2.2) but are similar to the periods of the surface pressure waves identified through wave number filtering, suggesting that the observed surface pressure signals are associated with similar surface waves. It is also apparent that the no-TC periods show some power in the low-frequency range, with peaks (although much weaker) at similar frequencies. This may indicate that other low-frequency waves are generated naturally in the tropics due to less organized convection or other dynamical processes. Regardless, the power spectra from the buoy data show clear evidence that gravity waves generated by TCs can be detected by surface instruments.

During the observing periods, the intensities of Chaba, Fanapi, and Megi were 110–115 knots, 75–90 knots, and 145–155 knots, respectively, and they were 235–345 km, 240–260 km, and 340–360 km from the buoy. With the limited data available at this time, it is not possible to test or derive a relationship between power

**4. Comparison to Surface Observations**

**4.1. Buoy Data and Processing**

To determine if the surface pressure signals seen in the numerical simulations can be observed in the real atmosphere, we turn to surface wind and pressure data collected by the Extreme Air-Sea Interaction (EASI) buoy that was designed to directly measure air-sea fluxes and mean properties of the air-sea interface in high wind and wave conditions [Drennan *et al.*, 2014]. The EASI buoy was moored for 3 months during the 2010 Pacific typhoon season as part of the Impact of Typhoons on the Ocean in the Pacific (ITOP) experiment [D’Asaro *et al.*, 2014]. Three typhoons, Fanapi, Megi, and Chaba, passed by the EASI buoy in 2010 [see Potter *et al.*, 2015, Figure 4]. We selected three periods when the typhoon centers were 150–400 km away from the buoy. For comparison, we also selected three periods of similar duration when no TC was near the buoy. Table S2 summarizes the start and end time of each of the six periods. Note that the surface wind and pressure data were originally recorded with sampling rate of 10 Hz (for turbulent flux measurements), but data with 0.1 Hz sampling rate were used in the present analysis.

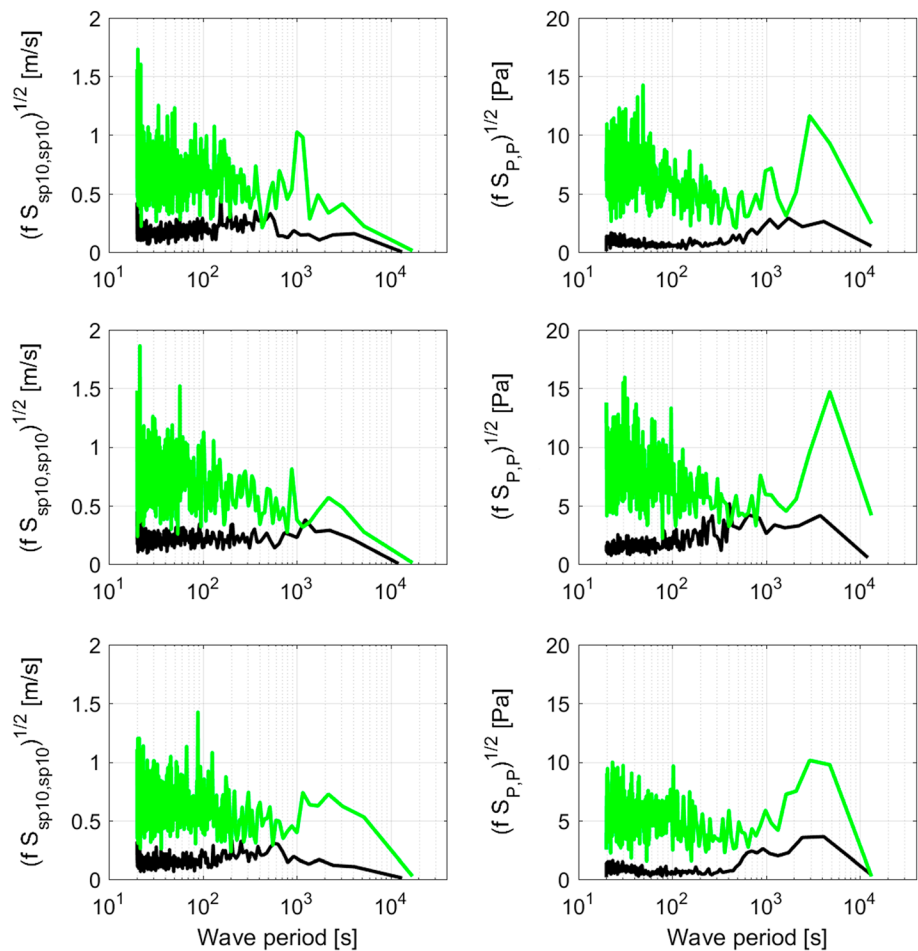


**Figure 5.** Power spectra (green curves) of surface pressure and surface wind speeds observed by the ITOP buoy in the Pacific in 2014 during the passage of Typhoons (top) Chaba, (middle) Fanapi, and (bottom) Megi, for (left column) wind speed and (right column) surface pressure. Included in each figure is a power spectrum from a similar time period where no TC was nearby (black curves).

spectral density, distance, and TC intensity as suggested by the model output. Nonetheless, the similarities in the shapes of the low-frequency ends of power spectra from the model output and the buoy are encouraging. While the simulated wind amplitudes are an order of magnitude too low, the simulated pressure amplitudes are very similar.

## 5. Conclusions

Observers have noted the generation of gravity waves from TCs for several decades, with most attention given to deep, long-wavelength waves that also propagate into the stratosphere. This paper shows that TCs also continuously radiate shorter waves that are wrapped into tight spirals. These waves can be observed by satellite images, research aircraft, and surface instruments. The flight level data reveal waves with radial wavelengths of 2–10 km, and by compositing the data from inbound and outbound flight legs separately, an outward phase speed of 20–25  $\text{ms}^{-1}$  can be inferred. Data from a research buoy in the Pacific also show evidence for the effects of the gravity waves on surface pressure and wind speed, with periods around 1000 s and 2000 s.

Numerical simulations reproduce these waves and suggest that the waves at flight level and at the surface are distinct, with different scales and frequencies. The simulations also indicate that TC intensity can be correlated with the amplitudes of these wave signals, including those observed at the surface. This suggests that, perhaps, in some geographic regions, networks of surface instruments could monitor the intensity of

approaching or passing TCs, much as the worldwide network of seismometers continuously monitors earthquakes. Interestingly, some recent studies have shown evidence for detectable seismic waves from TCs and other weather systems via the pressure forces associated with large ocean waves [Gerstoft *et al.*, 2006; Nishida and Takagi, 2016]. Analysis of atmospheric gravity waves may be a more direct approach for remote monitoring of TC intensity.

#### Acknowledgments

The authors thank M. Onderlinde for performing the idealized TC simulations, H. Graber and N. Williams for providing the ITOP data, and B. McNoldy for providing the satellite images. D. Nolan was supported by the NSF through grant AGS-1132646 and by NOAA through grant NA14NWS4680028; J. Zhang was also supported by NA14NWS4680028. The model output used in this simulation is available through an anonymous transfer site hosted by the Center for Computational Sciences at the University of Miami; access information can be provided by the authors. Flight level data are available from the Hurricane Research Division of NOAA through their website at [http://www.aoml.noaa.gov/hrd/data\\_sub/hurr.html](http://www.aoml.noaa.gov/hrd/data_sub/hurr.html), and processed data can also be obtained from the authors. Data from the ITOP campaign can be accessed at [http://data.eol.ucar.edu/master\\_list?project=ITOP](http://data.eol.ucar.edu/master_list?project=ITOP).

#### References

- Aberson, S. D., M. L. Black, R. A. Black, J. J. Cione, C. W. Landsea, and F. D. Marks Jr. (2006), Thirty years of tropical cyclone research with the NOAA P-3 aircraft, *Bull. Am. Meteorol. Soc.*, *87*, 1039–1055.
- Black, P. G. (1983), Tropical storm structure revealed by stereoscopic photographs from Skylab, *Adv. Space Res.*, *2*(6), 115–124, doi:10.1016/0273-1177(82)90131-4.
- Black, P. G., E. A. D'Asaro, W. M. Drennan, J. R. French, P. P. Niiler, T. B. Sanford, E. J. Terrill, E. J. Walsh, and J. A. Zhang (2007), Air-sea exchange in hurricanes: Synthesis of observations from the Coupled Boundary Layer Air-Sea Transfer experiment, *Bull. Am. Meteorol. Soc.*, *88*, 357–374.
- Corbosiero, K. L., and J. Molinari (2003), The relationship between storm motion, vertical wind shear, and convective asymmetries in tropical cyclones, *J. Atmos. Sci.*, *60*, 366–376, doi:10.1175/1520-0469(2003)060<0366:TRBSMV>2.0.CO;2.
- D'Asaro, E. A., et al. (2014), Impact of typhoons on the ocean in the Pacific, *Bull. Amer. Meteor. Soc.*, *95*, 1405–1418, doi:10.1175/BAMS-D-12-00104.1.
- Drennan, W. M., H. C. Graber, C. O. Collins III, A. Herrera, H. Potter, R. J. Ramos, and N. J. Williams (2014), EASI: An Air–Sea Interaction Buoy for High Winds, *J. Atmos. Oceanic Tech.*, *31*, 1397–1409, doi:10.1175/JTECH-D-13-00201.1.
- Union, J. P. (2011), Re-writing the climatology of the tropical North Atlantic and Caribbean Sea atmosphere, *J. Clim.*, *24*, 893–908, doi:10.1175/2010JCLI3496.1.
- Durrant, D. R., and J. A. Weyn (2016), Thunderstorms do not get butterflies, *Bull. Am. Meteorol. Soc.*, *97*, 237–244.
- Emanuel, K. A. (1991), The theory of hurricanes, *Annu. Rev. Fluid Mech.*, *23*, 179–196, doi:10.1146/annurev.fl.23.010191.001143.
- Gerstoft, P., M. C. Fehler, and K. G. Sabra (2006), When Katrina hit California, *Geophys. Res. Lett.*, *33*, L17308, doi:10.1029/2006GL022720.
- Jewtoukoff, V., R. Plougonven, and A. Hertzog (2013), Gravity waves generated by deep tropical convection: Estimates from balloon observations and mesoscale simulations, *J. Geophys. Res. Atmos.*, *118*, 9690–9707, doi:10.1002/jgrd.50781.
- Japan Meteorological Agency (2016), New geostationary meteorological satellites—Himawari 8/9. [Retrieved November 2016 from [http://www.jma.go.jp/jma/jma-eng/satellite/news/himawari89/himawari89\\_leaflet.pdf](http://www.jma.go.jp/jma/jma-eng/satellite/news/himawari89/himawari89_leaflet.pdf)].
- Kim, S.-Y., H.-Y. Chun, and D. L. Wu (2009), A study on stratospheric gravity waves generated by Typhoon Ewinia: Numerical simulations and satellite observations, *J. Geophys. Res.*, *114*, D22104, doi:10.1029/2009JD011971.
- Koch, S.-E., and L. M. Siedlarz (1999), Mesoscale gravity waves and their environment in the central United States during STORM-FEST, *Mon. Weather Rev.*, *127*, 2854–2879, doi:10.1175/1520-0493(1999)127<2854:MGWATE>2.0.CO;2.
- Markowski, P., and Y. Richardson (2010), *Mesoscale Meteorology in Mid-Latitudes*, chap. 6, pp. 161–180, Wiley-Blackwell, Hoboken, N. J.
- Molinari, J., P. Duran, and D. Vollaro (2014), Low Richardson number in the tropical cyclone outflow layer, *J. Atmos. Sci.*, *71*, 3164–3179, doi:10.1175/JAS-D-14-0005.1.
- Moon, Y., and D. S. Nolan (2015), Spiral rainbands in a numerical simulation of Hurricane Bill (2009). Part II: Propagation of inner rainbands, *J. Atmos. Sci.*, *72*, 191–215.
- Nastrom, G. D., and K. S. Gage (1985), A climatology of atmospheric wavenumber spectra of wind and temperature obtained by commercial aircraft, *J. Atmos. Sci.*, *42*, 950–960, doi:10.1175/1520-0469(1985)042<0950:ACOWS>2.0.CO;2.
- Nguyen, L., J. Molinari, and D. Thomas (2014), Evaluation of tropical cyclone center identification methods in numerical models, *Mon. Weather Rev.*, *142*, 4326–4339, doi:10.1175/MWR-D-14-00044.1.
- Niranjan Kumar, K., C. H. Kanaka Rao, A. Sandeep, and T. N. Rao (2014), SODAR observations of inertia-gravity waves in the atmospheric boundary layer during the passage of tropical cyclone, *Atmos. Sci. Lett.*, *15*, 120–126, doi:10.1002/asl2.478.
- Nishida, K., and R. Takagi (2016), Teleseismic S wave microseisms, *Science*, *353*, 919–921, doi:10.1126/science.aaf7573.
- Nolan, D. S. (2011), Evaluating environmental favorableness for tropical cyclone development with the method of point-downscaling, *J. Adv. Model. Earth Syst.*, *3*, M08001, doi:10.1029/2011MS000063.
- Nolan, D. S., and M. G. McGauley (2012), Tropical cyclogenesis in wind shear: Climatological relationships and physical processes, in *Cyclones: Formation, Triggers, and Control*, edited by K. Oouchi and H. Fudeyasu, pp. 1–36, Nova Sci. Publ., Hapauge, New York, doi:10.1007/s00221-012-3059-y.
- Nolan, D. S., Y. Moon, and D. P. Stern (2007), Tropical cyclone intensification from asymmetric convection: Energetics and efficiency, *J. Atmos. Sci.*, *64*, 3377–3405, doi:10.1175/JAS3988.1.
- Onderlinde, M. J., and D. S. Nolan (2016), Tropical cyclone-relative environmental helicity and the pathways to intensification in shear, *J. Atmos. Sci.*, *73*, 869–890, doi:10.1175/JAS-D-15-0261.1.
- Potter, H., H. C. Graber, N. J. Williams, C. O. Collins III, R. J. Ramos, and W. M. Drennan (2015), In situ measurements of momentum fluxes in typhoons, *J. Atmos. Sci.*, *72*, 104–118.
- Sato, K. (1993), Small-scale wind disturbances observed by the MU radar during the passage of Typhoon Kelly, *J. Atmos. Sci.*, *50*, 518–537, doi:10.1175/1520-0469(1993)050<0518:SSWDOB>2.0.CO;2.
- Stephan, C. C., M. J. Alexander, M. Hedlin, C. D. De Groot-Hedlin, and L. Hoffman (2016), A case study on the far-field properties of propagating tropospheric gravity waves, *Mon. Weather Rev.*, *144*, 2947–2961, doi:10.1175/MWR-D-16-0054.1.
- Sutherland, B. R. (2010), *Internal Gravity Waves*, chap. 1, pp. 1–73, Cambridge Univ. Press, New York.
- Vallis, G. K. (2006), *Atmospheric and Oceanic Fluid Dynamics*, chap. 2, pp. 51–122, Cambridge Univ. Press, Cambridge, U. K.
- Yue, J., S. D. Miller, L. Hoffman, and W. C. Straka III (2014), Stratospheric and mesospheric concentric gravity waves over tropical cyclone Mahasen: Joint AIRS and VIIRS satellite observations, *J. Atmos. Solar-Terrestrial Phys.*, *119*, 83–90, doi:10.1016/j.jastp.2014.07.003.
- Zhang, J. A. (2010), Spectral characteristics of turbulence in the hurricane boundary layer over the ocean between the outer rainbands, *Q. J. R. Meteorol. Soc.*, *136*, 918–926, doi:10.1002/qj.610.
- Zhang, J. A., and W. M. Drennan (2012), An observational study of vertical eddy diffusivity in the hurricane boundary layer, *J. Atmos. Sci.*, *69*, 3223–3236, doi:10.1175/JAS-D-11-0348.1.